Rheol Acta (2002) 41: 211–222

ORIGINAL CONTRIBUTION

Tobias Roths
Christian Friedrich
Michael Marth
Josef Honerkamp*

Dynamics and rheology of the morphology of immiscible polymer blends – on modeling and simulation

Received: 25 September 2000
Accepted: 24 April 2001

T. Roths (✉) · C. Friedrich · M. Marth
J. Honerkamp
Albert-Ludwigs-Universität
Freiburger Materialforschungszentrum
Stefan-Meier-Str. 21
79104 Freiburg im Breisgau, Germany
e-mail: roths@fmf.uni-freiburg.de

* Extra address:
Albert-Ludwigs-Universität
Fakultät für Physik
Hermann Herder-Str. 3
79104 Freiburg im Breisgau, Germany

Abstract The material properties of heterogeneous polymer blends are crucially influenced by their morphology, i.e., by the spatial structure of the blend components and by the specific configuration of the interfaces separating the phases. Hence, in order to understand the behavior of experimentally obtained morphologies, one is interested in modeling the relevant dynamics of the morphology subject to external flow. Thus one can study, e.g., through the interfacial stress tensor the rheological properties due to the interfaces. The balance equations used for that purpose are based on a Cahn-Hilliard equation for the local concentration, the continuity equation, and a modified Navier-Stokes equation for the local velocity. The essential material and processing parameters such as surface tension, viscosity and volume fraction of both polymers, and imposed shear rate are taken into consideration as model coefficients. By regarding hydrodynamic interaction, which is proved to be important in case of immiscible blends, the interfacial relaxation is described properly. Simulations in both three and two dimensions agree at least qualitatively with experimental results concerning droplet deformation, droplet coalescence, and interfacial rheological properties of the blend.

Key words Polymer blends · Morphology · Cahn-Hilliard equation · Navier-Stokes equation · Coalescence · Interfacial rheological properties

Introduction

Blending of different polymers is a common method of creating new materials with certain desired material properties. In particular, if the blend components are standard polymers blending is much more economic than designing and synthesizing new homopolymers.

If the polymer components are not miscible but segregated into distinct spatial regions called phases the polymer blend is denoted as *immiscible* or *heterogeneous*, reflecting the fact that the blend shows a mesoscale structure denoted as (phase) *morphology*. Thus, the morphology reveals the *spatially varying local concentrations*, i.e., local volume fractions of the polymer components. It is a special feature of heterogeneous blends that their material properties – specifically their rheological behavior – not only depend on the properties of the blend components but also on the blend morphology (see, e.g., Paul and Newman 1978; Han 1980; Utracki 1989; Vinckier et al. 1996).

In the case of *dispersion morphology*, spherical particles of one component are dispersed in the continuous phase of the other polymer which is macroscopically extended and hence denoted as matrix. Accordingly, the blend properties are dominated by the matrix polymer. With increasing volume fraction the dispersed phase

finally percolates and becomes continuous, too. The phases of both polymer components interpenetrate each other and constitute a so-called three-dimensional interpenetrating phase network. Thus, this *bi-* or *cocontinuous* morphology is suitable for combining the properties of the two polymers properly.

However, it is not only the topology of the phases which has a great impact on the rheological behavior but also the configuration of the interfaces separating the phases. The macroscopic stress tensor contains a contribution, denoted as *interfacial stress tensor*, which is proportional to the anisotropy of the interfaces (cf. Bachelor 1970). For morphologies with complex interfaces, Doi and Ohta (1991) have derived semiphenomenological kinetic equations describing the time evolution of the interfacial area and its anisotropy in a given flow field. Accordingly, these equations could be suitable for describing the dynamics of the interfacial stress tensor and thus the rheological properties due to the interfaces. For that, however, one has to make *explicit* assumptions on the interfacial relaxation. In particular, one has to specify empirical relaxation times which depend in unknown manner on the configuration of the interfaces (i.e., on the morphology).

Hence, in this paper the dynamics of the morphology itself, i.e., of the local concentrations of the blend components, are considered instead. Thus, the elementary processes of morphology formation such as deformation due to external flow and interfacial relaxation, which is mainly driven by hydrodynamic interaction in case of immiscible blends (see, e.g., Bray 1994), are *implicitly* specified through known material and processing parameters.

The model equations discussed in the section Model equations are based on the Cahn-Hilliard balance equation for the local concentration of the polymer components (Cahn and Hilliard 1958) enhanced by an external velocity term, the continuity equation, and a modified Navier-Stokes equation. The latter equation takes into account the hydrodynamic fluctuations of the velocity field due to the interfaces, which have been neglected by Ohta et al. (1990). The resulting system of partial differential equations which complies with model H of the classification introduced by Hohenberg and Halperin (1977) includes the essential material and processing parameters like surface tension, viscosity and volume fraction of both polymers, and imposed shear rate. In contrast to interface tracking methods as boundary element methods (for BEM see, e.g., Rallison 1980; Khayat et al. 1997) the interfaces are not modeled explicitly but given implicitly by the concentration field, i.e., by the morphology. Hence, changes in the topology of complex interfaces such as the reconnections that appear during coalescence will not cause any difficulties.

Alternative approaches of modeling blends may be Molecular Dynamics (for a comparison to numerical integration of the corresponding balance equations, corresponding to above ansatz, see Furukawa 1997) or Immiscible Lattice Gas or Lattice Boltzmann methods (for an overview refer to Rothman and Zaleski 1997). However, in the case of immiscible blends, where one is not interested in the microscopic fluctuations, and with simple geometries of the integration range, the ansatz discussed in this paper may be favorable since then numerical integration is more efficient.

In the section Numerical implementation, fast algorithms are outlined for the numerical integration in both three and two spatial dimensions. With that it is possible to investigate the evolution of the morphology in consideration of hydrodynamic interaction *and* in case of externally applied shear.

Finally, the section Simulation results indicates that simulations can contribute to the understanding of both morphology formation and interfacial rheological properties of immiscible blends. By simulating the deformation of a single droplet and comparing it with theoretical results (Taylor 1934) it is demonstrated that interfacial relaxation is described properly. Furthermore, shear-induced coalescence is simulated in the case of dispersion morphology and compared with observations of Börschig et al. (2000a, b). Finally, the dependence of the interfacial rheological behavior on the specific morphology is investigated by means of the interfacial stress tensor, thus supporting the findings of Steinmann et al. (2000) that blend elasticity increases significantly at the transition from dispersion to cocontinuous morphology.

Model equations

In order to describe the relevant dynamics of morphology the following section discusses the balance equations for the local concentration and the local velocity of the polymer components. On a mesoscopic scale of order of the interfacial width but much larger than the polymer molecules these quantities are treated as continuous variables, i.e., they will change continuously over the interfaces. On this scale the polymer characteristics, and hence the model coefficients, will be determined by kinematic quantities as the viscosity or the diffusion coefficient.

Continuity equation for the local concentrations

As pointed out above, the morphology reflects the local concentrations, i.e., the local volume fractions $c_{A/B}$ ($c_A + c_B = 1$) of the polymer components A, B. Accordingly the dynamics of either of these quantities has to be modeled. In this paper the difference $\phi = c_{A-}c_B = 2c_{A-1}$ is considered instead, which is

consistent with other publications in the field of phase separation.

In order to comply with mass-conservation law for both polymer components A and B, i.e., in order to conserve the global concentrations ($\Phi_{A/B} = \int d^3r\, c_{A/B} = const.$), the following balance equation for $\phi = \phi(\mathbf{r}, t)$ is necessary and sufficient:

$$\frac{\partial}{\partial t}\phi + \nabla \cdot [\phi \mathbf{v}] + \nabla \cdot \mathbf{j}_\phi = 0 \ . \tag{1}$$

Here, $\mathbf{v} = \mathbf{v}(\mathbf{r},t)$ denotes the local velocity of the element of fluid at position $\mathbf{r}$ and time t and $\mathbf{j}_\phi$ stands for the diffusion flow due to dissipation. The term $\nabla \cdot [\phi \mathbf{v}]$ models the convection of the morphology by the underlying flow field which gives rise to an influence of $\mathbf{v}$ on ϕ.

For the diffusion flow the common constitutive equation is used, i.e., $\mathbf{j}_\phi$ is assumed to be proportional to the gradient of the local chemical potential μ:

$$\mathbf{j}_\phi = -M \nabla \mu_\phi \ , \tag{2}$$

with the proportionality factor M denoted as mobility or Onsager coefficient. In this equation M is assumed to be constant and independent of ϕ, i.e., $M[\phi] \equiv M_0$, which is an appropriate approximation for both the first and the very late stages of phase separation. In the first case the local concentrations are still quite homogeneous, i.e., $\phi \approx 0$, and thus indeed $M[\phi] \approx M_0$. In the latter case the phases are already well separate according to immiscible blends. Here, the diffusion just keeps the phases separated but the dynamics of the morphology, and in particular interfacial relaxation, is mainly driven by convection flow due to hydrodynamic interaction (cf., e.g., Bray 1994). Hence, the dependence of M on ϕ, generally the explicit form of Eq. (2) is not very crucial, provided that it keeps the phases separated. To complete the picture it should be mentioned that in the intermediate stages of phase separation, when the phases are partly separated, coarsening is still driven by diffusion and the above approximation probably will be oversimplifying (see, e.g., Sappelt and Jäckle 1998).

Using the phenomenological Cahn-Hilliard free energy (Cahn and Hilliard 1958) the chemical potential, which is given by the variational derivative $\mu_\phi(\mathbf{r},t) = \delta F / \delta \phi\ (\mathbf{r},t)$ of the free energy of the system F with respect to ϕ, reads

$$\mu_\phi = -a\phi + b\phi^3 - K\nabla^2\phi \ , \tag{3}$$

with positive model coefficients a, b, and K the meaning of which is discussed in the following.

The equilibrium concentrations are given by the minima of F, i.e., by $\mu_\phi = 0$. The polynomial part of μ_ϕ yields two stable uniform concentrations $\phi_\pm = \pm\sqrt{a/b}$. Accordingly, in order to obtain the immiscible case, i.e., $\phi_\pm = \pm 1$ corresponding to $c_A = 1$ and $c_A = 0$ respectively far from the interfaces, it has to be $a = b$.

The Laplacian $\nabla^2\phi$ in Eq. (3) penalizes the occurrence of interfaces where ϕ changes rapidly and thus models the influence of the interfacial energy on diffusion. Hence, the nonuniform equilibrium concentration with a planar interface normal to the x direction (satisfying the boundary conditions $\phi\,(x = \pm\infty) = \pm 1$) is given by $\phi_e(x) = \tanh(\sqrt{2K/a})$. Thus, according to the experimental reality, the interfaces (implicitly given by $\phi = 0$) have a small but finite width

$$d = 2\sqrt{K/a} \ . \tag{4}$$

Furthermore, in the case of a planar interface the interfacial energy σ, which is equal to the excess energy due to the interfaces, is given by

$$\sigma = K \int_{-\infty}^{+\infty} dx \left[\frac{d}{dx}\phi_e\right]^2 = \frac{2\sqrt{2Ka}}{3} \ . \tag{5}$$

Accordingly, by solving these equations it is possible to express the model coefficients $a = b$ and K by the measurable material parameters d and σ.

In order to substitute the remaining coefficient M (cf. Eq. 2) by an experimentally accessible quantity, too, one may linearize Eqs. (1), (2), and (3) around the equilibrium concentration ϕ_+. Thus, one obtains the common diffusion equation of component B in A with the corresponding diffusion coefficient being $D_{AB} = 2M_0 a$. Accordingly, M can be inferred from D_{AB} which is accessible by experiment.

Finally, in order to get dimensionless quantities of order one, length, velocity, and time are scaled by the characteristic length chosen as the interfacial width d (typically of order 5 nm), the characteristic velocity v_0 (specified by the shear velocity of order $\dot{\gamma}d$), and the resulting characteristic time $t_0 = d/v_0$. Thus, the characteristic quantities are chosen with regard to the interfacial width d, which constitutes the smallest characteristic length scale of the physical system. Other characteristic length scales are the characteristic domain size D of the morphology, i.e., the mean sphere size in case of spherical morphologies, and the flow domain L for which the following relations hold: $d \ll D \ll L$ (the first inequality holds at least in case of separated phases, i.e., of immiscible blends, which is addressed in this paper). In order to capture the real physics of polymer blends, all characteristic length scales should be resolved by the numerical simulation (as much as possible). Accordingly, the above scaling is suitable for the numerical implementation since the spacing of the numerical grid is related to the interfacial width d (cf. section Numerical implementation). However, the above inequalities give rise to some serious problems concerning the numerical simulation. In order to resolve D and L one has to use very large grid sizes and/or restrict oneself to the investigation of effects where these quantities may be

assumed as not too large (cf. also section Numerical implementation).

Rescaling Eqs. (1), (2), and (3) in this way one obtains the final equation for ϕ:

$$\frac{\partial}{\partial t}\phi + \nabla \cdot [\phi \mathbf{v}] = \mathrm{Pe}^{-1}\nabla^2 \mu'_\phi \quad \text{with}$$
$$\mu'_\phi = -\phi + \phi^3 - \frac{1}{4}\nabla^2 \phi \tag{6}$$

and the Péclet number which reads $\mathrm{Pe} = 2\frac{v_0 d}{D_{\mathrm{AB}}}$ using the above scaling. This partial differential equation is supplemented with two balance equations for the local velocity $\mathbf{v}$ resulting from the laws of mass and momentum conservation.

Continuity equation for the total density

Without being too restrictive the blend components are assumed to have equal densities and the blend is taken as incompressible. Thus, the blend density ρ is considered as spatially and temporally constant and the general continuity equation $\frac{\partial}{\partial t}\rho + \nabla \cdot [\rho \mathbf{v}] = 0$ resulting from mass-conservation reduces to

$$\nabla \cdot \mathbf{v} = 0 \ , \tag{7}$$

i.e., the velocity field $\mathbf{v}$ is required to be source-free.

Balance equation for the total momentum

In order to obtain momentum conservation a generalized Navier-Stokes equation is assumed for $\mathbf{v}$:

$$\rho\left[\frac{\partial}{\partial t}\mathbf{v} + (\mathbf{v}\cdot\nabla)\mathbf{v}\right] = -\nabla p + \nabla \cdot [\eta \dot{\boldsymbol{\gamma}}] + \mu_\phi \nabla \phi \ .$$

Here, p is the local pressure and η stands for the shear viscosity which may depend on ϕ, though we restrict ourselves to the isoviscous case $\eta_{\mathrm{A}} = \eta_{\mathrm{B}} = \eta$ in the following. The stress tensor depends linearly on the local shear rate $\dot{\boldsymbol{\gamma}} = \nabla \mathbf{v} + \nabla \mathbf{v}^{\mathrm{T}}$. Accordingly, the blend is considered as a mixture of Newtonian fluids, i.e., the elastic properties are not taken into account for the components. However, for small (smaller than the smallest inverse relaxation time of the bulk phases) and stationary shear rates as considered below this simplification is not too restrictive. Furthermore, below we focus on the elastic properties due to the interfaces, which are dominant especially if the blend components are rather inelastic.

The additional capillary term $\mu_\phi \nabla \phi$ which contains the interfacial tension σ through the chemical potential (cf. Eqs. 3 and 5) models the capillary forces at the interfaces: In the limit of vanishing interface width d and limited curvature of the interface c ($dc \to 0$) it renders a force proportional to σ and to c (see, e.g., Kawasaki 1977). These modifications of the Navier-Stokes equation take into account the *hydrodynamic interaction*, the influence of ϕ respectively the morphology on $\mathbf{v}$, and thus describe the spatial variations of the velocity field due to the interfaces.

Using the scaling introduced in the preceding section (cf. Eq. 6) in order to obtain dimensionless variables of order one, above equation finally reads

$$0 \approx \mathrm{Re}\left[\frac{\partial}{\partial t}\mathbf{v} + (\mathbf{v}\cdot\nabla)\mathbf{v}\right] = -\nabla p + \nabla \cdot [\eta \dot{\boldsymbol{\gamma}}] + C\mu'_\phi \nabla \phi \ , \tag{8}$$

with the Reynolds number $Re = v_0 d\rho/\eta$ and $C = 6\sigma/\eta v_0$ being two dimensionless coefficients which again can be inferred from measurable material parameters. For high-viscous matter such as polymers and moderate velocities the Reynolds number and thus the left-hand side of Eq. (8) are several orders of magnitude smaller than the right-hand side (which is of the order of one). Accordingly, the inertial force (given by the left-hand side) can be neglected so that the velocity $\mathbf{v}$ is instantaneously inferable from ϕ. For this purpose it may be favorable to decompose the velocity into two contributions $\mathbf{v} = \mathbf{v}_{\mathrm{hom}} + \mathbf{v}_{\mathrm{inhom}}$: here, $\mathbf{v}_{\mathrm{hom}}$ stands for the *externally* imposed macroscopic flow field. This part which is independent of ϕ would be the resulting flow field if the blend was homogeneous. Accordingly, since this contribution is known in advance it just remains to calculate $\mathbf{v}_{\mathrm{inhom}}$ denoting the *internal* spatial variations of the velocity field due to hydrodynamic interaction, which is adjusted independent of the externally imposed flow field. From the mathematical point of view this corresponds to the fact that every solution ($\mathbf{v}$) of a linear inhomogeneous partial differential equation (PDE) such as Eq. (8) (with the capillary term representing the inhomogeneity and the pressure p being determined by the incompressibility condition at Eq. 7) can be reduced to one particular solution ($\mathbf{v}_{\mathrm{hom}}$) of the corresponding *homogeneous* PDE (i.e., without the capillary term) and another solution ($\mathbf{v}_{\mathrm{inhom}}$) of the whole, *inhomogeneous* PDE.

Scope of the model equations

The discussed system of partial differential equations (PDE) (Eqs. 6, 7, and 8) is capable of describing the dynamics of polymer blends in the case of separated phases, i.e., of immiscible blends, as well as phase separation of an initially homogeneous blend that starts demixing by spinodal decomposition due to thermodynamic instability (Gunton et al. 1983). These dynamics can be investigated subject to an externally imposed macroscopic flow field which has to be specified by the boundary conditions (e.g., simple shear) *and* in consideration of hydrodynamic interaction.

Hydrodynamic interaction may only be neglected in the special cases of constant viscosity η and $C \approx 0$ (corresponding to vanishing interfacial tension or extremely large viscosities) or $\phi \approx 0$ (i.e., at the beginning of phase separation when the blend is still quite homogeneous). Then, the fluctuations due to hydrodynamic interaction vanish ($\mathbf{v}_{\text{inhom}} \equiv 0$). Equations (7) and (8) decouple from Eq. (6) so that the velocity is entirely determined by the macroscopic flow field ($\mathbf{v} = \mathbf{v}_{\text{hom}}$), e.g., in case of shear by a linear velocity profile according to the applied shear rate $\dot{\gamma}_{\text{appl}}$. Hence, given this velocity field which is temporally constant and independent of ϕ only the diffusion equation (Eq. 6) has to be integrated as done by Ohta et al. (1990).

Generally, however, the hydrodynamic interaction is expected to be of great importance and must not be neglected (see, e.g., Bray 1994). This is especially the case for immiscible blends where the phases are well separated. In this instance, which is addressed in this paper, the velocity strongly depends on ϕ so that the entire system of differential equations has to be integrated simultaneously, greatly increasing the numerical effort required.

Numerical implementation

In the following section a solver is outlined for the system of PDE (Eqs. 6, 7, and 8). In particular, integration range and grid, boundary conditions, and numerical implementation are specified for the case of shear flow. However, the numerics is easily modifiable in order to simulate other relevant flow such as elongational flow.

Numerical integration is performed on a cubic integration range with the integration grid chosen as static and square with N_x, N_y, and N_z equidistantly distributed grid points in the x, y, and z direction. A static, equidistant grid is given preference to adaptive grids which are fine-meshed at the interfaces where ϕ changes rapidly but large-meshed elsewhere and are often used with finite element methods (FEM). In case of complex morphologies subject to external flow field (as investigated below) one cannot really take advantage of these grids since they had to be adopted continuously to the convected morphology which increases the numerical expenditure. The grid spacing Δx is equated to the interfacial width d (being 1 after the scaling introduced above) which is proved to be fine enough in order to prevent numerical artifacts due to the discreteness such as "pinning" of the morphology to the underlying grid.

Boundary conditions are specified assuming shear flow with the flow direction defining the x-axis and the shear gradient plane being the x-y plane: In the x and z directions periodic boundary conditions are employed for the variables ϕ and $\mathbf{v}_{\text{inhom}}$ but sheared periodic boundary condition in the y direction as used by Ohta et al. (1990). That is to say a gridpoint (x,y,z) is identified with the points $(x + N_x,y,z)$ and $(x,y,z + N_z)$, but also with $(x + \gamma N_y,y + N_y,z)$ where $\gamma(t) = \int_0^t \dot{\gamma}_{\text{appl}}(t')\mathrm{d}t'$ is the applied shear strain at time t.

In order to investigate immiscible blends with rather coarse morphologies and domain sizes up to 1 μm the grid size has to be at least 10^3 grid points per spatial dimension. With the interfacial width respectively the grid spacing being typically $\Delta x \approx 5$ nm this corresponds to physical dimensions of the integration range of about 5 μm which allows one to simulate complex morphologies with domain sizes up to 0.5–1 μm without boundary effects (which, however, are still rather small values). With these grid sizes, however, numerical integration is only feasible in two spatial dimensions (2D) for which reason the major part of below simulations is restricted to the x–y or shear gradient plane. Accordingly, besides a 3D solver a very efficient 2D solver is proposed in the following.

Numerical integration breaks down into two tasks: to infer $\mathbf{v}_{\text{inhom}}$ from ϕ by solving Eq. (8) subject to the incompressibility condition (Eq. 7) at given time t and, given $\mathbf{v} = \mathbf{v}_{\text{hom}} + \mathbf{v}_{\text{inhom}}$, to integrate the convection–diffusion equation (Eq. 6) in time.

Calculation of the velocity from ϕ

Differential equation Eq. (8) can be solved in Fourier space. Assuming the viscosity η as independent of ϕ one gets (the pressure p is eliminated by the condition Eq. (7)

$$\mathbf{v}_{\text{inhom}}(\mathbf{k}) = \mathbf{T}(\mathbf{k}) \cdot [\mathbf{C}\mu'_\phi \nabla\phi](\mathbf{k}) \ , \tag{9}$$

where the argument $\mathbf{k}$ indicates the Fourier transform of the corresponding quantity. In particular

$$\mathbf{T}(\mathbf{k}) = \frac{1}{\eta k^2}\left(1 + \frac{\mathbf{k}\mathbf{k}}{k^2}\right) \tag{10}$$

denotes the Fourier transform of the Oseen tensor $\mathbf{T}(\mathbf{r})$ (Kawasaki 1977). Transferred into real space the matrix operation in Eq. (9) becomes a convolution integral for $\mathbf{v}_{\text{inhom}}(\mathbf{r},t)$:

$$\mathbf{v}_{\text{inhom}}(\mathbf{r},t) = \int \mathrm{d}\mathbf{r}'\mathbf{T}(\mathbf{r}-\mathbf{r}')[C\mu'_\phi\nabla\phi](\mathbf{r}',t)$$
$$\text{with } \mathbf{T}(\mathbf{r}) = \frac{1}{8\pi\eta r}\left(1 + \frac{\mathbf{r}\mathbf{r}}{r^2}\right) \tag{11}$$

the calculation of which is numerically not feasible. Accordingly, the calculation is performed in Fourier space using fast Fourier transform (FFT) for the transformations (for the FFT algorithm refer to, e.g., Press et al. 1992).

However, this procedure implies periodic boundary conditions in all directions. Accordingly, in case of differing boundary conditions (as in the case of shear) the calculated velocity field will be distorted at the boundaries of the integration range. These distortions, however, will diminish with increasing distance from the boundaries and finally vanish.

Accordingly, this shortcoming can be overcome by extending the integration range and continuing the dynamic variable ϕ according to the real boundary conditions. In order to meet the above boundary conditions introduced for shear flow, a cubic range is added at both the lower and the upper boundary in the y direction and ϕ is continued sheared periodically into this range. Then, the calculated velocity will still be distorted at the upper and lower boundary of the thus *extended* integration range. If the extension is large enough, however, these distortions will be restricted to the extension, but within the original integration range $\mathbf{v}_{\mathrm{inhom}}$ will be calculated correctly, i.e., will comply with sheared periodical boundary conditions in the y direction.

For the 2D simulations in the x–y (shear gradient) plane the following, more efficient solver for Eq. (8) may be favorable. In order to fulfill the incompressibility condition (Eq. 7) it is convenient to introduce a stream function $\psi = \psi(\mathbf{r},t)$ as

$$\mathbf{v}_{\mathrm{inhom}} = \nabla \times (\psi\hat{\mathbf{z}}) = \frac{\partial}{\partial \mathbf{y}}\psi\hat{\mathbf{x}} - \frac{\partial}{\partial \mathbf{x}}\psi\hat{\mathbf{y}} \ , \tag{12}$$

where $\hat{\mathbf{x}}$ and $\hat{\mathbf{y}}$ stand for the unit vectors in x respectively y direction, whereas $\hat{\mathbf{z}}$ is the unit vector normal to the 2D integration plane. Accordingly, the components of the velocity $\mathbf{v}_{\mathrm{inhom}}$ are specified by $v_x = \frac{\partial}{\partial y}\psi$, $v_y = -\frac{\partial}{\partial x}\psi$ and above (sheared) periodic boundary conditions hold for ψ as well (as for $\mathbf{v}_{\mathrm{inhom}}$).

Taking the curl of Eq. (8) and inserting Eq. (12) yields an inhomogeneous biharmonic partial differential equation (Chella and Viñals 1996),

$$\nabla^4\psi = C(\nabla\mu_\phi \times \phi)\cdot\mathbf{z} \ , \tag{13}$$

where the inhomogeneity on the right-hand side is determined by ϕ. From this equation one can infer ψ and thus $\mathbf{v}$ by means of a fast biharmonic solver as proposed by Bjørstad (1980). This solver requires a cubic integration range and explicit boundary conditions, i.e., the values of ψ and of its normal derivative $\frac{\partial}{\partial n}\psi$ have to be specified explicitly at the boundaries of the integration range. However, if one assumes the above (sheared) periodic boundary conditions for ψ, these values are not known explicitly in advance. This difficulty can be overcome as in the 3D case. The integration range is extended in the y as well as in the x direction and ψ is continued consistently into this range. Furthermore, the boundary values for the *extended* integration range may be approximated by the corresponding values inferred from the solution ψ of the preceding integration time step. Then, the distortions due to this approximation will be restricted to the narrow vicinity of the boundary of the *extended* integration range, i.e., to the extension. Accordingly, within the original range the calculated ψ and thus $\mathbf{v}_{\mathrm{inhom}}$ will comply again with (sheared) periodic boundary conditions (if the extension is chosen sufficiently large).

Integration of ϕ

In order to integrate the convection–diffusion equation (Eq. 6) in time an explicit finite difference scheme is used that fits in the cell dynamic approach introduced by Oono and Puri (1988). In order to stabilize numerics, convection term and diffusion term are integrated separately in two steps:

$$\tilde{\phi}_t = \phi_t + \Delta t[-\nabla\cdot[\phi_t\mathbf{v}_t]] \ , \tag{14}$$

$$\phi_{t+\Delta t} = \tilde{\phi}_t + \Delta t\left[\mathrm{Pe}^{-1}\nabla^2\left(\phi_t + \phi_t^3 - \frac{1}{4}\nabla^2\phi_t\right)\right] \tag{15}$$

according to Shinozaki and Oono (1993). Thus, given ϕ_{t} and $\mathbf{v}_{\mathrm{t}} = \mathbf{v}_{\mathrm{hom,t}} + \mathbf{v}_{\mathrm{inhom,t}}$, which in turn is inferable from ϕ_{t} as pointed out in the preceding section, one can calculate $\phi_{\mathrm{t}+\Delta\mathrm{t}}$ at the next time step $t + \Delta t$.

For the calculation of the right-hand sides of above equations, strictly speaking for the calculation of ∇ and ∇^2, the above (sheared) periodic boundary conditions are applied. In order to reduce anisotropy effects caused by the discrete integration grid the center difference scheme is applied for the convection term $\nabla\cdot[\phi\mathbf{v}]$. Furthermore, the Cartesian Laplacian ∇^2 of the diffusion term is discretized as isotropic as possible.

Alternative approaches

Instead of using finite difference schemes for the integration of Eqs. (6, 7, and 8), finite element methods (FEM) may also be employed. These methods (used by, e.g., Anderson et al. 1999) differ in the way the original continuous equations are transferred into discrete approximations.

A conceptually different approach is to establish and simulate microscopic dynamics which obey on a coarse-grained, mesoscopic scale the relevant balance equations (such as Eqs. 6, 7, and 8). These microscopic dynamics may be borrowed from reality as in case of Molecular Dynamics (for a comparison between molecular dynamics and numerical integration of the corresponding balance equation in case of spinodal decomposition see Furukawa 1997) or be rather artificial as in case of

Immiscible Lattice Gas or Lattice Boltzmann methods (for an overview concerning these methods refer to Rothman and Zaleski 1997).

These methods are very flexible and especially advantageous if complex geometries have to be considered or if one focuses on the microscopic fluctuations which may be interesting in the first stages of phase separation. Otherwise, integrating directly the corresponding balance equation may be favorable since then the numerical algorithm is more efficient.

Simulation results

The following simulations of isoviscous immiscible blends were performed using typical values of the material parameters listed in Table 1 (these quantities are used through the model coefficients Pe, Re and C as discussed in section Model equations). According to Wu (1982) the chosen values are characteristic of the model system PS/PMMA (investigated, e.g., by Börschig et al. 2000a, b; Steinmann et al. 2000). In the following figures white and black corresponds to local concentrations $\phi = 1$ (pure component A) and $\phi = -1$ (pure component B) respectively.

Interfacial relaxation

At first, it will be proved that the above balance equations (Eqs. 6, 7, and 8) describe correctly the relaxation of the interfaces. For this purpose the deformation of a droplet is simulated and compared with the well-established predictions due to Taylor (1934). In shear flow a droplet becomes an ellipsoid. For isoviscous blends at steady state, i.e., when deformation due to the externally imposed shear flow and interfacial relaxation balance one another, the deformation parameter $D = (l - s)/(l + s)$ is related to the capillary number $\mathrm{Ca} = \eta\dot{\gamma}R_0/\sigma$ according to (Taylor 1934)

$$D = \frac{35}{32}\mathrm{Ca} \ . \tag{16}$$

Here, l, s denote, respectively, the longest and shortest axes of the ellipsoid in the shear gradient plane and R_0 is the radius of the undeformed droplet. The relation at Eq. (16) is exact in the limit of vanishing deformations and holds in good approximation for $D < 0.3$.

Table 1 Material parameters used for the simulations

ρ	σ	$\eta_A = \eta_B$	$d(=\Delta x)$
1×10^3 kg/m^3	2×10^{-3} N/m	1×10^4 Pa s	5×10^{-9} m

The simulations are performed in 3D with a grid size of 128^3. The droplet radius is chosen as 30 grid points (corresponding to $R_0 = 150$ nm) which is large enough in order to neglect effects due to the finite interfacial width as well as sufficiently small in order to avoid wall effects due to the finite integration range. As can be seen in Fig. 1 the deformation parameters obtained from simulations with different shear rates (error bars) correspond well with the theoretical prediction at Eq. (16) which proves the usefulness of the balance equations discussed in section Model equations. The error bars in Fig. 1 result from the errors in estimating l and s respectively.

Regarding this, it should be mentioned that interface tracking methods as boundary element methods (for BEM see, e.g., Rallison 1980; Khayat et al. 1997) may be more appropriate for the above investigations. However, due to an explicit parameterization of the interfaces, these methods will fail when there are changes of the interfacial topology such as breakup or coalescence. Integrating the balance equations (Eqs. 6, 7, and 8) circumvents these problems. The interfaces are not modeled explicitly but considered just implicitly which makes this method very robust and therefore more favorable in case of complex morphologies (i.e., in case of complex geometries of the interfaces) as they are discussed below (see Figs. 4, 5, 6, 7, and 8).

As pointed out in section Numerical implementation, simulations of complex morphologies are only feasible in two dimensions. Accordingly, it is investigated whether interfacial relaxation behaves appreciably different in 2D or not. In order to do this, the behavior of a 2D droplet with a diameter of 150 grid points corresponding to 750 nm is considered. For two different shear rates $\dot{\gamma} = 0.01\,\mathrm{s}^{-1}, \dot{\gamma} = 0.1\,\mathrm{s}^{-1}$, Fig. 2a, b shows the steady-state deformation taken at shear strain $\gamma = 3$. Again, the deformation parameters obtained from the simulations (listed in Table 2) correspond at least qualitatively with the theoretical predictions of

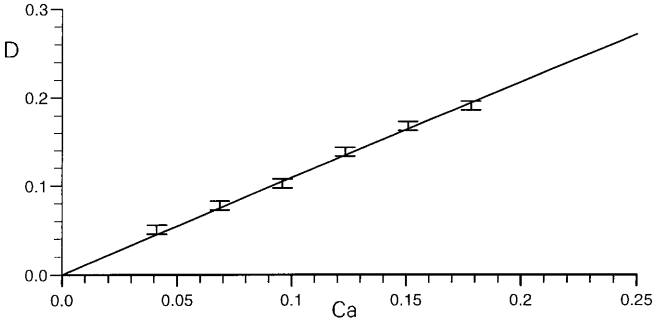

Fig. 1 Deformation of a droplet subject to shear flow. The *error bars* mark the steady-state deformation parameter D obtained from the 3D simulations in dependence on the capillary number *Ca*. The *solid line* stands for the theoretical prediction at Eq. (16) due to Taylor (1934)

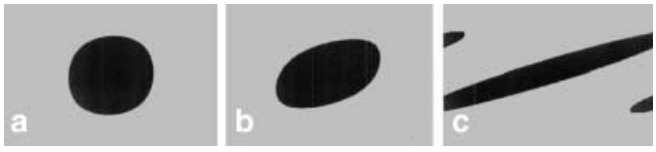

Fig. 2a–c Deformation of a 2D droplet with diameter 750 nm subject to shear flow with a shear rate of: **a** $\dot{\gamma} = 0.01\,\mathrm{s}^{-1}$; **b** $\dot{\gamma} = 0.1\,\mathrm{s}^{-1}$ at shear strain $\gamma = 3$ (corresponding to steady state). Neglecting hydrodynamic interaction (**c**) the droplet is highly deformed even with small shear rate $\dot{\gamma} = 0.01\,\mathrm{s}^{-1}$ (deformation has still not reached its steady state at strain $\gamma = 3$ which is shown in **c**)

Eq. (16). This may be interpreted as a hint that even 2D simulations of the morphology dynamics will contribute to the understanding of morphology formation, i.e., it warrants transferring the results of the below simulations to 3D.

Finally, Fig. 2 demonstrates the dominant influence of hydrodynamic interaction on interfacial relaxation. If hydrodynamic interaction is neglected, corresponding to $C = 0$ in Eq. (8), the remaining relaxation mechanism is due to diffusion (modeled by the diffusion term $\nabla \cdot \mathbf{j}_\phi$ in Eq. 1). However, in the case of separate phases this mechanism is substantially weaker as demonstrated in Fig. 2c. Even with small shear rates ($\dot{\gamma} = 0.01\,\mathrm{s}^{-1}$) interfacial relaxation due to diffusion is not able to counteract the deformation caused by shear flow so that the droplet is stretched excessively (and deformation has still not reached its steady state at strain $\gamma = 3$ which is displayed in Fig. 2c). Accordingly, this proves that the real relaxation process of the interfaces is essentially governed by convection flow due to hydrodynamic interaction. That is to say with hydrodynamic interaction the underlying velocity field is influenced characteristically by the morphology. Hence, if the sphere is deformed the velocity field is adjusted in such a manner that it neutralizes the external flow field in the vicinity of the sphere and thus prevents further deformation.

Shear-induced coalescence

In order to investigate shear-induced coalescence, i.e., domain growth under shear flow, dispersion morphologies have been generated on a 1000^2 grid with concentrations of the disperse component of $\Phi_A = 5\%$. The initial size distribution of the dispersed particles has been chosen quite narrow with an average diameter of 20 grid points (corresponding to 100 nm with a grid spacing of 5 nm as listed in Table 1). This value has been proven to be sufficiently large in order to avoid distortions due to the discrete integration grid.

Table 2 Deformation of a droplet subject to shear flow: deformation parameter obtained from 2D simulations (Fig. 2) compared with the theoretical predictions due to Taylor (Eq. 16)

	$\dot{\gamma} = 0.01\,\mathrm{s}^{-1}$	$\dot{\gamma} = 0.1\,\mathrm{s}^{-1}$
D (simulation)	0.044	0.30
D (due to Taylor 1934)	0.041	0.41

Figure 3 shows the evolution of the mean sphere size (diameter $d(\gamma)$) for different shear rates $\dot{\gamma} = 0.02\,\mathrm{s}^{-1}$, $0.1\,\mathrm{s}^{-1}$, $0.2\,\mathrm{s}^{-1}$, and $1.0\,\mathrm{s}^{-1}$ in dependence on total strain γ. For each shear rate the mean sphere size has been inferred from the first zero of the correlation function averaged over five independent simulations starting from different initial morphologies. The simulations have been terminated at a shear strain of $\gamma = 80$ in order to prevent distortions due to boundary effects which may occur when the particle size becomes larger than ≈1/10 of the integration size.

For all shear rates one can observe coalescence caused by shear-induced collision and subsequent merging of dispersed particles. Furthermore, one can take from Figs. 4, 5, and 6 that coalescence broadens the size distribution, i.e., increases the variance of the particle sizes as reported by, e.g., Börschig et al. (2000b). If one disregards the smallest shear rate $\dot{\gamma} = 0.02\,\mathrm{s}^{-1}$ the domain size increases approximately in a linear manner. This would be in agreement with the results of Börschig et al. (2000a) reported for "hard" spheres, where the viscosity of the disperse phase has been more than one order of magnitude larger than the matrix viscosity ("hard" means, that the spheres are not deformed by the shear flow itself, neither do they get deformed on collision). In this instance the averaged domain size actually scales with γ, with the constant growth rate being independent of the shear rate. That is to say, the kinetics of coalescence is the same if the time is rescaled with the characteristic time of the system which is given by the inverse shear rate $\dot{\gamma}^{-1}$.

However, in contrast to the latter finding the final growth rates of the simulations shown in Fig. 3 rather decrease with increasing shear rate (cf. also Figs. 4, 5, and 6). On the other hand, this result agrees with observations of, e.g., Börschig et al. (2000b) who found

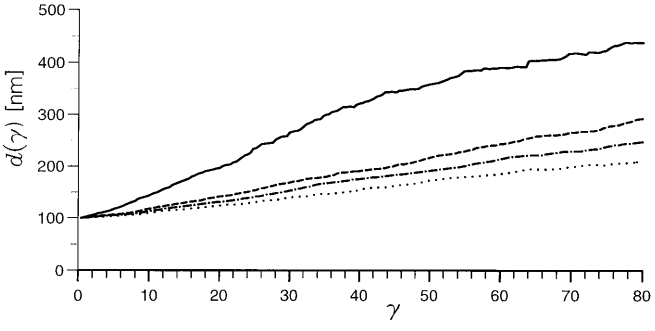

Fig. 3 Shear-induced coalescence: Average particle size in dependence on shear strain for different shear rates $\dot{\gamma} = 0.02\,\mathrm{s}^{-1}$ (——), $0.1\ \mathrm{s}^{-1}$ (- - - - -), $0.2\ \mathrm{s}^{-1}$ (-·-·-), and $1.0\ \mathrm{s}^{-1}$ (· · · · ·)

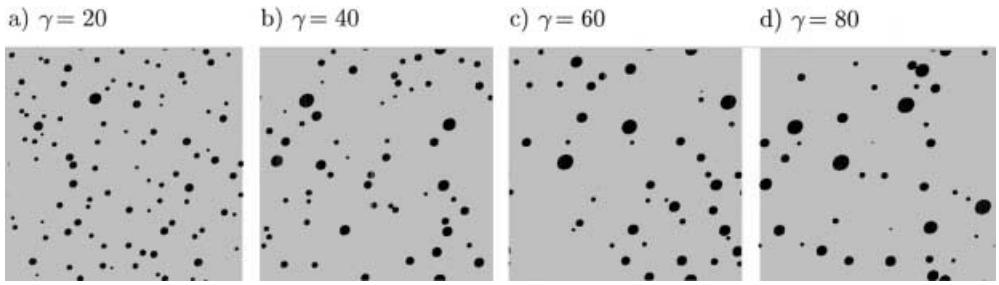

Fig. 4 Coalescence of simulated morphologies ($\Phi_A = 5\%$): evolution of the mean sphere size (diameter $d(\gamma)$) for shear rate $\dot{\gamma} = 1.0\,s^{-1}$ in dependence on total strain γ. The initial sphere size distribution is narrow with an average sphere size of about 100 nm

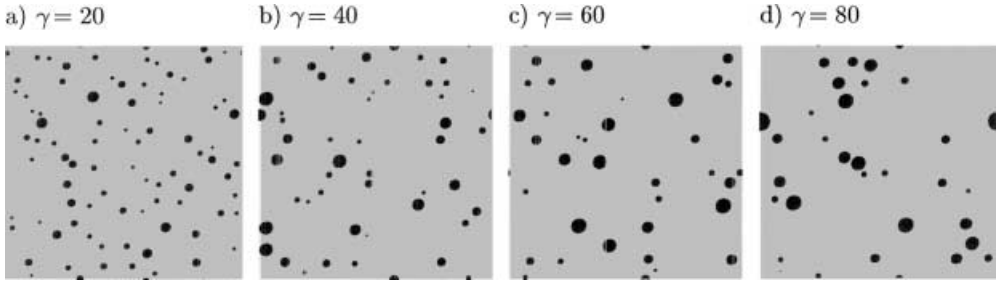

Fig. 5 Coalescence of simulated morphologies ($\Phi_A = 5\%$): evolution of the mean sphere size (diameter $d(\gamma)$) for shear rate $\dot{\gamma} = 0.1\,s^{-1}$ in dependence on total strain γ. The initial morphology (at $\gamma = 0$) is the same as in Fig. 4

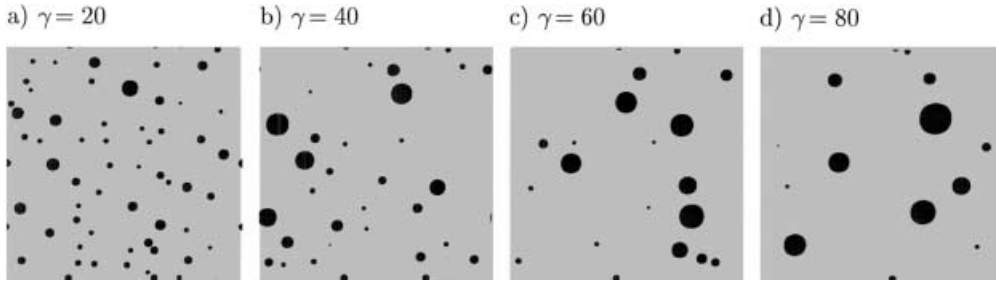

Fig. 6 Coalescence of simulated morphologies ($\Phi_A = 5\%$): Evolution of the mean sphere size (diameter $d(\gamma)$) for shear rate $\dot{\gamma} = 0.02\,s^{-1}$ in dependence on total strain γ. The initial morphology (at $\gamma = 0$) is the same as in Fig. 4

that coalescence can be tremendously suppressed in case of "soft" particles (in this case the viscosity of the disperse phase has been approximately one order of magnitude smaller than the matrix viscosity).

These findings can be explained as follows. With increasing shear rate the spheres finally get deformed as can be observed in Figs. 4, 5, and 6. And even if the spheres are not deformed significantly by the shear flow itself, they nevertheless can get deformed during collision, and the curve the higher the shear rate and the larger the sphere size (due to the larger influence of interfacial relaxation small drops do not deform that easily, as can be inferred from, e.g., Eq. 16). Then, however, the separating matrix film is larger and accordingly drains very slowly. Thus, rather than draining away the separating matrix film, colliding particles may pass each other without merging. Hence, the probability for shear induced collisions and thus coalescence (in dependence on shear strain γ) are reduced with increasing shear rate.

Despite these quantitative differences the curves in Fig. 3 are quite similar for $\dot{\gamma} = 0.1\,s^{-1}, \dot{\gamma} = 0.2\,s^{-1}$, and $\dot{\gamma} = 1.0\,s^{-1}$. In the case of the smallest shear rate $\dot{\gamma} = 0.02\,s^{-1}$, however, coalescence seems to behave different: For small shear strains ($\gamma < 40$) coalescence is significantly enhanced whereas for $\gamma > 40$ the corresponding curve in Fig. 3 shows the same growth rate as the curve of the larger shear rate $\dot{\gamma} = 0.1\,s^{-1}$. This can be explained as follows. First, as has been discussed above, coalescence is known to be the more reduced the larger the particles are. Accordingly, this effect will result in decreasing growth rates as the shear strain γ and accordingly the particle size increase. Furthermore, one can derive from the simulations that for very small shear rates and small particle sizes (and sufficiently large concentration of the disperse phase) the internal fluctuations of the velocity field due to hydrodynamic interaction $\mathbf{v}_{\text{inhom}}$ become larger than (or at least of the order of) the shear gradient of the external shear flow $\mathbf{v}_{\text{hom}}$. Accordingly, self-induced coalescence, which is driven by these internal fluctuations, enhances further shear-induced coalescence caused by the external shear field. However, the influence of self-induced coalescence seems to vanish

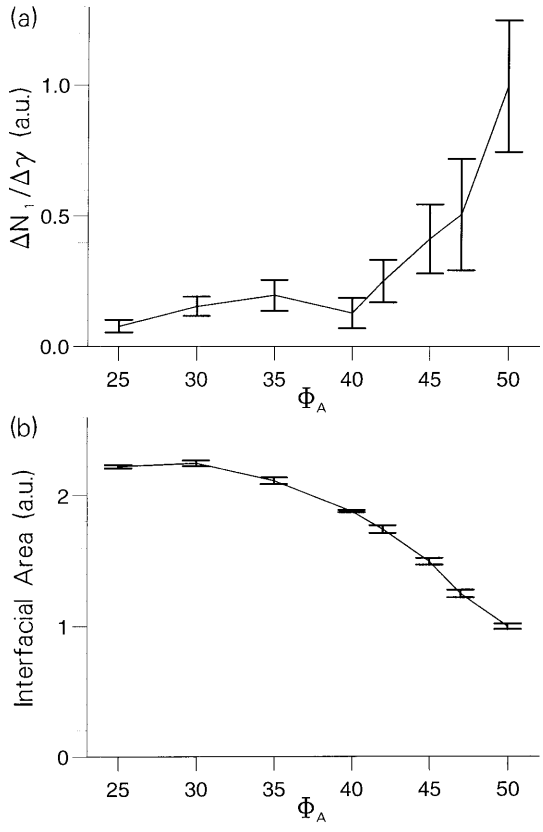

Fig. 7a, b Interfacial elasticity: **a** $\Delta N_1/\Delta\gamma$ ($\Delta\gamma = 0.1$); **b** interfacial area in dependence on the concentration Φ_A (scaled with respect to the corresponding value for $\Phi_A = 50\%$). For every concentration the results are averaged over 16 independent simulations. Due to the symmetry with respect to an exchange of component A and B it is sufficient to consider the range $\Phi_A \leq 50\%$

(at least in 2D) with increasing particle size as the shear gradients induced by the internal fluctuations $\mathbf{v}_{\text{inhom}}$ decrease and finally become smaller than the shear gradient of the external shear flow $\mathbf{v}_{\text{hom}}$.

Finally it should be mentioned that the simulated growth rates are about twice as large as the ones observed by Börschig et al. (2000a). Most likely this discrepancy is due to the different dimensionality of real experiment and simulation. In three dimensions two colliding particles have more topological possibilities of evading each other, i.e., of avoiding coalescence. Accordingly, it is not astonishing that the simulations do not correspond exactly with the experimental results. However, at least qualitatively the simulations reveal the same effects as discussed above.

Rheological properties due to the interfaces

Finally, the rheological properties due to the interfaces are addressed. In particular, the relation between elasticity and blend morphology is investigated. The simulation results are compared with experimental findings of Steinmann et al. (2000). Especially for isoviscous blends elasticity is found to increase significantly at the phase inversion point (i.e., at the transition from dispersion to cocontinuous morphology) and therefore can serve as rheological classifier for phase inversion.

Generally, the rheological properties can be inferred from the kinetics of the macroscopic stress tensor which for isoviscous blends is given by (Bachelor 1970):

$$\sigma_{\alpha\beta} = p\delta_{\alpha\beta} + \eta\dot{\gamma}_{\alpha\beta} + \sigma q_{\alpha\beta} \quad . \tag{17}$$

Here, η is the shear viscosity disregarding the influence of the interfaces, and p and σ denote the pressure respectively the interfacial tension. Furthermore it is $\dot{\gamma}_{\alpha\beta} = \partial_\beta \bar{v}_\alpha + \partial_\alpha \bar{v}_\beta$ where $\partial_\beta \bar{v}_\alpha$ are the components of the of the macroscopic velocity gradient tensor (cf. Eq. 8). Additionally

$$q_{\alpha\beta} = \frac{1}{V}\int \mathrm{d}S\left(n_\alpha n_\beta - \frac{1}{3}\delta_{\alpha\beta}\right) \tag{18}$$

stands for the anisotropy of the interfaces. In this surface integral which runs over all the interfaces, V denotes the total system volume and n_α stands for the unit vector normal to the interfaces. When the interfacial thickness is sufficiently small the following relation (Eq. 19)

$$q_{\alpha\beta} \propto \int \mathrm{d}^3 r(\partial_\alpha \phi)(\partial_\beta \phi) \tag{19}$$

can be used to infer the anisotropy from simulated morphologies ϕ.

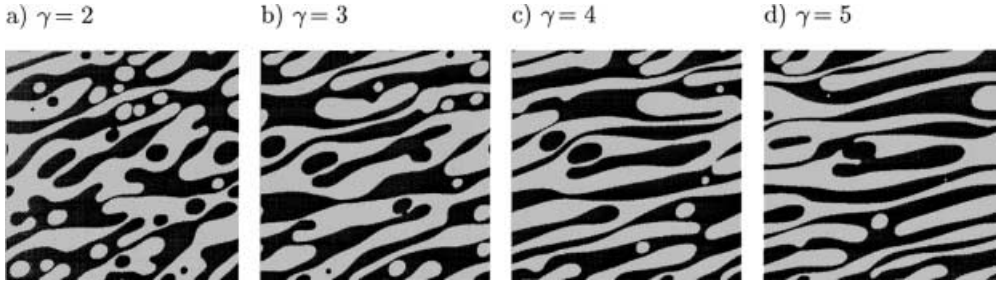

Fig. 8a–d Simulated morphology with concentration $\Phi_A = 50\%$: Cocontinuous morphology for shear rate $\dot{\gamma} = 0.1\,\mathrm{s}^{-1}$ at: **a** $\gamma = 2$; **b** $\gamma = 3$; **c** $\gamma = 4$; **d** $\gamma = 5$. On the right of (b) and (c) one can observe the occurrence of breakup

Accordingly, in case of heterogeneous blends the spatial anisotropy tensor at Eq. (18) gives rise to an excess shear stress due to the interfaces and thus describes the interfacial rheological properties in dependence on ϕ. In particular, the interfacial elasticity is characterized by the increase of the first normal stress difference $N_1 = \sigma\ (q_{yy} - q_{xx})$ with respect to a small applied shear strain $\Delta\gamma$, i.e., by $\Delta N_1/\Delta\gamma$ (where $\Delta\gamma(t) = \dot{\gamma} \cdot \Delta t$, with $\dot{\gamma} \to 0$ and thus $\Delta\gamma \to 0$) which is displayed in Fig. 7a.

This quantity is investigated in dependence on the blend morphology. Therefore, on a 1000^2 grid both dispersion and cocontinuous morphologies have been generated by varying the concentration Φ_A (due to the symmetry of the problem $\Phi_B = 1 - \Phi_A$ it is sufficient to consider concentrations $\Phi_A \leq 50\%$). For $\Phi_A < 40\%$ dispersion morphologies are obtained, above $\Phi_A \approx 40\%$ the domains tend to percolate, i.e., they form interconnected structures of "macroscopic" extent (strictly speaking they extend over the whole integration range as can be seen in Fig. 8) so that the morphology becomes gradually cocontinuous. Independent of the concentration Φ_A, the characteristic length of the simulated morphology inferred from the first zero of the correlation function (and identical with the mean sphere size in case of spherical morphologies) has been chosen as 20 grid points. This choice is large enough to be able to neglect effects due to the discrete integration grid as well as sufficiently small in order to avoid wall effects due to the finite integration range.

The interfacial area (shown in Fig. 7b) corresponds well with experimental findings of Luciani (2000) who observed a distinct minimum of the interfacial area at $\Phi_A = 50\%$. Accordingly, the enhancement of elasticity in the case of cocontinuous morphology ($\Phi_A > 40\%$ in Fig. 7a) does not correlate with an increased amount of interfacial area as one might suppose. That is to say it is not the absolute value of interfacial excess energy corresponding to the total amount of interfacial area which gives rise to elasticity.

Interfacial elasticity, which is quantified by $\Delta N_1/\Delta\gamma$ ($\Delta\gamma \to 0$) as pointed out above, rather corresponds to a change of interfacial stress, i.e., to a deformation of interfacial geometry caused by external strain. Due to the interconnected structures, however, a cocontinuous morphology is far more deformed by shear flow than a dispersion morphology as illustrated in Fig. 8 (in order to demonstrate more clearly the deformation, the strain applied on the morphology in Fig. 8 is very much larger than the small shear strain $\Delta\gamma$ in Fig. 7). In particular the deformation cannot be balanced by interfacial relaxation since the corresponding relaxation times diverge as the domains get macroscopically extended. Accordingly, though the droplets of a dispersion morphology give rise to an elastic behavior, too, interfacial elasticity is significantly enhanced in case of cocontinuous morphology (cf. Fig. 7).

Finally, apart from deformation, Fig. 8 reveals another effect influencing the formation of morphology: For instance in Fig. 8b, c (right part) one can observe the occurrence of breakup of coherent domains caused by shear which results in dissipation of energy. In the case of spherical morphology when the domains are not interconnected breakup occurs just for larger shear rates $\dot{\gamma} \gg 1\,\mathrm{s}^{-1}$ when the deformation of the spheres is sufficiently large. However, also in the case of cocontinuous morphology breakup is reduced due to hydrodynamic interaction. In particular the fibrillary structures depicted in Fig. 8 will be less stable if hydrodynamic interaction is neglected.

Concluding, the findings of Steinmann et al. (2000) that blend elasticity increases significantly at the phase inversion point are confirmed by the simulations and can be explained by the interfacial properties.

Conclusions

The material properties of immiscible polymer blends are decisively influenced by the morphology and in particular by the configuration of the interfaces. Accordingly, one is interested in modeling and simulating the relevant dynamics of morphology. The aim is to simulate the evolution of morphology subject to external flow. This in turn allows one to study the kinetics of the interfacial stress tensor (through the anisotropy tensor of the interfaces) and thus to infer the rheological properties due to the interfaces.

The model discussed in this paper consists of a system of balance equations for the local concentration difference and the local velocity. The model equations are capable of describing the dynamics in the case of separate phases, i.e., of immiscible blends, but also phase separation (spinodal decomposition) in consideration of external flow and hydrodynamic interaction. In the case of immiscible blends it has been proved by simulations that the equations describe properly both deformation of the morphology (due to the externally imposed flow field) and interfacial relaxation which is mainly driven by convection flow due to hydrodynamic interaction.

Concluding, it has been shown that the simulations can contribute to the understanding of both morphology formation and interfacial rheological properties of immiscible blends. For example, though restricted to two dimensions the simulations of droplet coalescence correspond at least qualitatively with experimental results. Furthermore, the simulations have been able to confirm experimental results concerning the relationship between blend morphology and blend elasticity. In particular the observed enhancement of blend elasticity

at the phase inversion point can be explained by a slowed interfacial relaxation in case of cocontinuous morphology.

Acknowledgments We gratefully acknowledge financial support by the Deutsche Forschungsgemeinschaft through the Sonderforschungsbereich 428.

References

Anderson PD, Galaktionov OS, Peters GWM, Vosse FN, Meijer HEH (1999) Analysis of mixing in three-dimensional cavity flows. J Fluid Mech 386:149–166

Bachelor GK (1970) The stress system in a suspension of force-free particles. J Fluid Mech 41:420–427

Bjørstad P (1980) In: Elliptic problem solvers II. Academic Press, New York

Börschig C, Arends B, Gronski W, Friedrich C (2000a) Kinetics of flow-induced coalescence and form relaxation in polymer blends as studies by rheo small angle light scattering. Macromol Symp 149:137–143

Börschig C, Fries B, Gronski W, Weis C, Friedrich C (2000b) Shear-induced coalescence in polymer blends – simulations and rheo small angle light scattering. Polymer 41:3029–3035

Bray AJ (1994) Theory of phase-ordering kinetics. Adv Phys 43:357–459

Cahn JW, Hilliard JE (1958) Free energy of a nonuniform system. I. Interfacial free energy. J Chem Phys 28:258–267

Chella R, Viñals J (1996) Mixing of a two-phase fluid by cavity flow. J Phys Rev E 53:3832–3840

Doi M, Ohta T (1991) Dynamics and rheology of complex interfaces. J Chem Phys 95:1242–1248

Furukawa H (1997) Dynamics of phase separation of a simple fluid mixture: comparison between molecular dynamics and numerical integration of the phenomenological equation. Phys Rev E 55:1150–1161

Gunton, JD, San Miguel M, Sahni PS (1983) Phase transitions and critical phenomena, vol 8. Domb C, Lebowitz JL (eds). Academic Press, New York

Han CD (1980) Multiphase flow in polymer processing. Academic, New York

Hohenberg PC, Halperin BI (1977) Theory of dynamic critical phenomena. Rev Mod Phys 49:435–479

Kawasaki K (1977) Theory of early stage spinodal decomposition in fluids near the critical point. I. Prog Theor Phys 57:826–839

Khayat RE, Luciani A, Utracki LA (1997) Boundary element analysis of planar drop deformation in confined flow. 1: Newtonian fluids. Eng Anal Bound Elem 20:279–289

Luciani A (2000) Private communications

Ohta T, Nozaki H, Doi M (1990) Computer simulations of domain growth under steady shear flow. J Chem Phys 93:2664–2675

Oono Y, Puri S (1988) Study of phase-separation dynamics by use of cell dynamical systems. I. Modeling. Phys Rev A 38:434–453

Paul S, Newman S (1978) Polymer blends, vol 1. Academic Press, San Diego

Press W, Teukolsky SA, Vetterling WT, Flannery BP (1992) Numerical recipes, vol 2. Cambridge University Press, New York

Rallison JM (1980) Note on the time-dependent deformation of a viscous drop which is almost spherical. J Fluid Mech 98:625–633

Rothman DH, Zaleski S (1997) Lattice-gas cellular-automata – simple models of complex hydrodynamics. Cambridge University Press, New York

Sappelt D, Jäckle J (1998) Percolation inversion in spinodal decomposition of mixtures with strong kinetic asymmetry. Polymer 39:5253–5256

Shinozaki A, Oono Y (1993) Spinodal decomposition in 3-space. Phys Rev E 48:2623–2654

Steinmann S, Friedrich C, Fahrländer M (2000) Morphological and rheological properties of selectively filled polymer blends with cocontinuous morphology. XIIIth International Congress on Rheology, 20–25th August 2000, Cambridge, UK, Proc 1:269–271

Taylor GI (1934) The formation of emulsions in definable fields of flow. Proc R Soc A 146:501–523

Utracki LA (1989) Polymer alloys and blends. Hanser Publisher, München

Vinckier I, Moldenaers P, Mewis J (1996) Relationship between rheology and morphology of model blends in steady shear flow. J Rheol 40:613–631

Wu S (1982) Polymer interface and adhesion. Dekker, New York